This work was written as part of one of the author's official duties as an Employee of the United States Government and is therefore a work of the United States Government. In accordance with 17 U.S.C. 105, no copyright protection is available for such works under U.S. Law.

Public Domain Mark 1.0
https://creativecommons.org/publicdomain/mark/1.0/

Access to this work was provided by the University of Maryland, Baltimore County (UMBC) ScholarWorks@UMBC digital repository on the Maryland Shared Open Access (MD-SOAR) platform.

Please provide feedback

Please support the ScholarWorks@UMBC repository by emailing scholarworks-group@umbc.edu and telling us what having access to this work means to you and why it’s important to you. Thank you.

Combining Remote and In-situ Sensing for Autonomous Underwater Vehicle Localization and Navigation

Cesar A. Rojas[1], Paulo V. Padrao[1], Jose E. Fuentes[1],
Arif R. Albayrak[2,3], Batuhan Osmanoglu[2], and Leonardo Bobadilla[1]

OCEANS 2022, Hampton Roads | 978-1-6654-6809-1/22/$31.00 ©2022 IEEE | DOI: 10.1109/OCEANS47191.2022.9977208

***Abstract*—Scientists continue to study the red tide and fish-kill events happening in Florida. Machine learning applications using remote sensing data on coastal waters to monitor water quality parameters and detect harmful algal blooms are also being studied. Unmanned Surface Vehicles (USVs) and Autonomous Underwater Vehicles (AUVs) are often deployed on data collection and disaster response missions. To enhance study and mitigation efforts, robots must be able to use available data to navigate these underwater environments. In this study, we compute a satellite-derived underwater environment (SDUE) model by implementing a supervised machine learning model where remote sensing reflectance (R_{rs}) indices are labeled with in-situ data they correlate with. The models predict bathymetry and water quality parameters given a recent remote sensing image. In our experiment, we use Sentinel-2 (S2) images and in-situ data of the Biscayne Bay to create an SDUE that can be used as a Chlorophyll-a map. The SDUE is then used in an Extended Kalman Filter (EKF) application that solves an underwater vehicle localization and navigation problem.**

***Index Terms*—remote sensing, machine learning, water quality, linear regression, estimation, autonomous underwater vehicle, chlorophyll-a, robots**

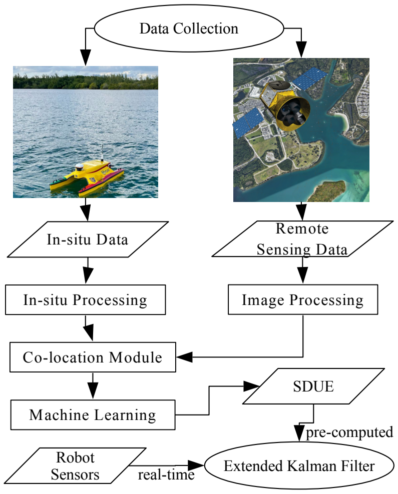

Fig. 1. Overview of our method for satellite-assisted robot localization.

I. INTRODUCTION

Localization in underwater environments is a central problem for autonomous vehicles (AUV), and it is a prerequisite needed for applications such as conservation of marine species, environmental monitoring, and infrastructure maintenance. However, traditional sensing modalities used for state estimation in outdoor robotics (e.g., GPS, compasses, LIDAR, and Vision) may be compromised in underwater scenarios. Our goal is to compute a satellite-derived underwater environment (SDUE) model (e.g., 3-D Chlorophyll and Bathymetry Map) and use it to solve an underwater robot localization and navigation problem. The AUV will rely on the widely used Extended Kalman filter (EKF) [1] to fuse information from the SDUE, GPS, and other sensors.

Figure 1 shows a flow chart illustrating our approach. We attempt to enhance the available in-situ data with remote sensing images captured by Sentinel-2 (S2) made available by the European Space Agency (ESA) and Sinergise Sentinel Hub for use in a supervised machine learning application. Our approach has the following caveat; we test our methodology using in-situ data without samples collected during a harmful water event. We also do not correct predicted values based on other water quality parameters such as turbidity.

II. RELATED WORK

Studies by Gholizadeh et al. [2], Nazeer et al. [3], Hafeez et al. [4], Cruz et al. [5] examine several approaches to applying statistical methods and machine learning algorithms with in-situ and remote sensing data and report metrics such as cross-validation accuracy scores and root-mean-square error (RMSE).

A. Satellite-Derived Bathymetry

Caballero et al. [6] derive bathymetry using S2 images of South Florida by calculating the pseudo-satellite-derived bathymetry or pSDB, labeling pSDB with bathymetry reference charts, and a linear regression model.

$$pSDB = \frac{\log(1000\pi R_{rs}(560))}{\log(1000\pi R_{rs}(492))} \tag{1}$$

---

[1] Cesar A. Rojas, Paulo V. Padrao, Jose E. Fuentes, and Leonardo Bobadilla are with the Florida International University Knight Foundation School of Computing and Information Sciences, Miami, FL 33199, USA (e-mail: croja022@fiu.edu, plope113@fiu.edu, jfuen099@fiu.edu, bobadilla@cs.fiu.edu)

[2] Arif R. Albayrak and Batuhan Osmanoglu are with the NASA Goddard Space Flight Center, Greenbelt, MD 20771, USA(e-mail:rustem.a.albayrak@nasa.gov, batuhan.osmanoglu@nasa.gov)

[3] Arif R. Albayrak is with the University of Maryland, Baltimore County, Baltimore MD 21228, USA(e-mail:albayrak@umbc.edu)

978-1-6654-6809-1/22/$31.00 ©2022 IEEE

Caballero et al. [7] further evaluate pSDB and study how water quality parameters such as turbidity and Chlorophyll-a affects the maximum predicted water column depth.

B. Satellite-Derived Chlorophyll-a

Mishra et al. [8] present the Normalized Difference Chlorophyll Index (NDCI) to estimate chlorophyll-a using remote sensing images of estuaries and coastal turbid waters.

$$NDCI = \frac{R_{rs}(704) - R_{rs}(665)}{R_{rs}(704) + R_{rs}(665)} \tag{2}$$

Caballero et al. [9] were able to use S2 images and NDCI to detect algal blooms in coastal waters, but use in-situ data to be able to detect harmful algal blooms caused by toxic algae species.

C. Satellite-Assisted Robot Navigation

Kodgule et al. [10] show how to use remote sensing and in-situ data in a Markov Decision Process for robot planetary exploration. The method relies on the spectral unmixing of lower resolution satellite data using higher resolution in-situ data collected during robot path navigation.

D. Underwater Localization

Due to the lack of GPS signals, accurate navigation continues to be a significant difficulty for any platforms traveling underwater [11]. Errors in the predicted position are caused by the process and sensor noise levels, which is crucial for autonomous underwater navigation [12]. In this context, the extended Kalman filter (EKF) is the most widely used navigation method to ensure precise localization underwater [13], [14], [15].

III. PROBLEM FORMULATION

A. Satellite-Derived Underwater Environment

We consider our ocean work environment as a 3-D environment denoted as $\mathcal{W} \subset \mathbb{R}^3$. Our workspace is then divided into a set of 2-D water layers at different depths. Assuming that the total number of water layers is denoted as L, the workspace $\mathcal{W}$ can be described as

$$\mathcal{W} = w_1 \cup w_2 \cup \cdots \cup w_L \tag{3}$$

At each layer $l \in \{1, \ldots, L\}$, the workspace w_l is modelled as $w_l \subset \mathbb{R}^2$ and we discretize the workspace into a 2-D grid. The free water space at each layer is denoted as

$$E_l = w_l \setminus O_l \tag{4}$$

where $O_l \subset \mathbb{R}^2$ is considered an inaccessible region for the underwater vehicle. Therefore, the free workspace is defined in terms of the entire workspace $\mathcal{W}$ as

$$\mathcal{E} = E_1 \cup E_2 \cup \cdots \cup E_L \tag{5}$$

Let $\mathcal{C}$ be the collection of all 2-D cells within a bounding convex polygon $\mathcal{P}$ where $\mathcal{P} \subseteq w_1$ represents our area of interest (AOI). Each cell has a center in the form of WGS84 coordinates denoted as (x, y, l), where $x, y \in \mathbb{R}$ describe longitude and latitude, and l with $0 \leq l \leq L$ describes water depth in meters. Each geographic coordinate (x, y) pair represents the center of an equal-sized grid tile that covers the resolution of the remote sensing data. Each unit of l values covers 1 meter in water depth.

Let $\mathcal{Q} = (d, b, i, m)$ be a satellite query configuration where d is a satellite identifier and b, i, m are lists of requested R_{rs} bandwidths, indices, and metadata respectively. Remote sensing data is denoted as $\rho : \mathcal{C} \times \mathcal{Q} \times T_1 \rightarrow \mathbb{R}^k$, where $T_1 = [0, t_1)$ is the collection time interval data and $k = |b| + |i| + |m|$ is the total number of variables.

Let $\beta : T_2 \rightarrow \mathbb{R}^n$ be the collection of all available in-situ data, where $T_2 = [0, t_2)$ represents the collection time interval and n is the number of in-situ sensors. The in-situ data collected on the surface by USVs is denoted as β_u.

Let $\mathcal{S} : \mathcal{W} \rightarrow \mathbb{R}^j$ be an SDUE computed by a supervised machine learning model, which uses the maps provided by ρ and β_u where values in ρ are labeled with values in β_u that share the same coordinates and a negligible difference in collection time and j is the number of predicted water parameters. The values labeled in ρ are in the form of a ratio or index that highly correlates to the in-situ data. At the center of each cell in the 3-D SDUE are the estimated in-situ measurements over a 10×10 meter area of one layer contained in $\mathcal{P}$

Problem 1: *Given an ocean work environment $\mathcal{W}$ of interest, a bounding convex polygon $\mathcal{P}$, a satellite configuration $\mathcal{Q}$, a collection of remote sensing data ρ, and a collection of in-situ data β, compute an SDUE $\mathcal{S}$.*

B. Vehicle Model

Our domain will have an AUV $\mathcal{A}$ at starting position $\mathbf{x}_0 = (x_0, y_0, 0) \in \mathcal{W}$. $\mathcal{A}$ collects in-situ data denoted as β_a. $\mathcal{A}$ can traverse $\mathcal{E}$ and move freely between layers. The AUV can be described by a discretized, non-linear system such that $f(\mathbf{x}_k, \mathbf{u}_k) + \mathbf{q}_k$ is the motion model of the vehicle where $\mathbf{x}_i$ is the state vector, and $\mathbf{u}_k$ input control vector, also the next state are related by $\mathbf{x}_{k+1} = f(\mathbf{x}_k, \mathbf{u}_k) + \mathbf{q}_k$ being $\mathbf{x}_0$ the initial position of the vehicle. $h(\mathbf{x}_k) + \mathbf{r}_k$ is the observation model of the vehicle, $\mathbf{q}_k$ and $\mathbf{r}_k$ are additive, zero-mean noise to account for model and sensing imperfections for each iteration k. We assume that $\mathcal{A}$ can be modeled as a rigid body and moves slowly at a constant speed v so that we can safely neglect its dynamics. We also assume that the water current is irrotational, having only horizontal linear velocity components. The sensors of $\mathcal{A}$ are composed of GPS, IMU (gyros, accelerometers), depth sensors, and water quality sensors. We describe $\mathcal{A}$ as a discretized, non-linear system as

$$\begin{aligned} \mathbf{x}_{k+1} &= f(\mathbf{x}_k, \mathbf{u}_k) + \mathbf{q}_k \\ \mathbf{z}_k &= h(\mathbf{x_k}) + \mathbf{r}_k \end{aligned} \tag{6}$$

such that $f(\mathbf{x}_k, \mathbf{u}_k)$ is the motion model of the vehicle, $h(\mathbf{x_k})$ is the observation model of the vehicle and z_k is the observation obtained by $\mathcal{A}$ at step k.

C. Motion Model

We assumed that the underwater vehicle can be modeled as a rigid body and that it is moving slowly at a constant speed v. Let $\mathcal{X}$ be the state space, i.e. the set of all possible states, and $\mathcal{U}$ be the action space, which represents the set of all possible actions. Therefore, at any given instant k, the vehicle can be described by

$$\begin{aligned} \mathbf{x}_k &= (x, y, l, \psi, v)^\top \in \mathcal{X} \\ \mathbf{u}_k &= (v, u_l, \omega)^\top \in \mathcal{U} \end{aligned} \tag{7}$$

in which (x, y) is the underwater horizontal position of the vehicle, l is the depth, ψ is the vehicle's heading, v is the vehicle's translational velocity, and ω is the angular velocity. Considering that u_l is an action that directly affects a change in depth, i.e $\dot{l} = u_l$, the simplified kinematic model of the vehicle is defined as

$$\mathbf{x}_{k+1} = \mathbf{A}\mathbf{x}_k + \mathbf{B}\mathbf{u}_k + \mathbf{q}_k \tag{8}$$

where the state transition matrix $\mathbf{A}$, the input matrix $\mathbf{B}$ are given by

$$\mathbf{A} = \begin{bmatrix} 1 & 0 & 0 & 0 & 0 \\ 0 & 1 & 0 & 0 & 0 \\ 0 & 0 & 1 & 0 & 0 \\ 0 & 0 & 0 & 1 & 0 \\ 0 & 0 & 0 & 0 & 0 \end{bmatrix}, \; \mathbf{B} = \begin{bmatrix} \Delta t \cos(\psi) & 0 & 0 \\ \Delta t \sin(\psi) & 0 & 0 \\ 0 & \Delta t & 0 \\ 0 & 0 & \Delta t \\ 1 & 0 & 0 \end{bmatrix} \tag{9}$$

and $\mathbf{q}_k$ is zero-mean noise distributed as $\mathbf{q}_k \sim \mathcal{N}(\mathbf{0}, \mathbf{Q}_k)$ with covariance given by

$$\mathbf{Q}_k = \begin{bmatrix} 1^2 & 0 & 0 \\ 0 & 1^2 & 0 \\ 0 & 0 & \left(\frac{\pi}{360}\right)^2 \end{bmatrix}$$

D. Observation Model

We assume that the vehicle sensors are composed of GPS, IMU (gyros, accelerometers), depth sensor, and water quality sensor (chlorophyll-a sensor) and that the vehicle can observe its state with uncertainties due to sensor imperfections and the dynamic nature of the underwater environment. Defining the observation space $\mathcal{Z}$ as the set of all possible sensor observations $\mathbf{z}_k \in \mathcal{Z}$ at iteration k, the observation model $h(\mathbf{x}_k)$ at the surface level given GPS and depth sensor readings are available can be represented by

$$\mathbf{z}_k = h(\mathbf{x}_k) = \begin{bmatrix} 1 & 0 & 0 & 0 & 0 \\ 0 & 1 & 0 & 0 & 0 \\ 0 & 0 & 1 & 0 & 0 \end{bmatrix} \mathbf{x}_k + \mathbf{r}_k \tag{10}$$

where $\mathbf{r}_k$ is zero-mean noise distributed as $\mathbf{r}_k \sim \mathcal{N}(\mathbf{0}, \mathbf{R}_k)$ with covariance given by

$$\mathbf{R}_k = \begin{bmatrix} 5^2 & 0 & 0 \\ 0 & 5^2 & 0 \\ 0 & 0 & 0.5^2 \end{bmatrix}.$$

When the vehicle is underwater, we use the 3-D SDUE to map chlorophyll-a measurements to locations given chlorophyll-a sensor data is available. Because of the uncertainty associated with the 3-D SDUE map construction, the deeper the vehicle descents, the higher the uncertainty is. In addition to that, there could be many $\mathbf{z}_k$ possible locations which have similar values to the measurements leading to inaccurate estimations. To address this issue, we consider a constrained (regularized) optimization problem to provide a reasonable candidate, let $\mathcal{S}$ the 3-D SDUE and $\mathbf{m}_k$ the measurement collected at step k and state $\mathbf{x}_k$. We define $g : \mathcal{W} \longrightarrow \mathcal{W}$ and $g(\mathbf{x}_k)$ as the solution to the optimization problem

$$\begin{aligned} \min_{\mathbf{x} \in \mathcal{W}} \quad & ||\mathcal{S}(\mathbf{x}) - \mathbf{m}_k||_2^2 \\ \text{s.t.} \quad & (\mathbf{x} - \mathbf{x}_k)^\top \mathbf{M}^{-1} (\mathbf{x} - \mathbf{x}_k) \leq 1. \end{aligned} \tag{11}$$

The matrix $\mathbf{M}$ is a positive definite matrix, which leads to a restriction in the sense of a Mahalanobis distance. In this case, we consider it a diagonal matrix. This restriction means that we are looking for places in the SDUE map whose measurements are close to the ones collected by the agent $\mathbf{m}_k$ within an ellipsoid centered at $\mathbf{x}_k$. We compute $\mathbf{z}_k$ in the same way as using the function h. Finally, it is possible to assume that g is a differentiable function by virtue of the implicit function theorem and the nature of the implied functions in Equation (11); nonetheless, its Jacobian was calculated using a finite difference scheme to estimate each partial derivative.

E. Extended Kalman Filter Framework

Consider the nonlinear system described in (6). The approximation used by the extended Kalman filter algorithm is based on truncated Taylor series expansion with the assumption that higher-order terms are negligible. The approximation of $f(\mathbf{x})$ is defined as

$$f(\mathbf{x}, \mathbf{u}) \approx f(\hat{\mathbf{x}}, \mathbf{u}) + \mathbf{F}\tilde{\mathbf{x}} \tag{12}$$

where $\mathbf{F}$ and $\mathbf{F}_k$ are the Jacobian derivatives of f respect to $\mathbf{x}$ evaluated at $(\hat{\mathbf{x}}, \mathbf{u})$ and $(\mathbf{x}_k, \mathbf{u}_k)$

$$\mathbf{F} = \frac{\partial f}{\partial \mathbf{x}}\bigg|_{(\hat{\mathbf{x}}, \mathbf{u})}, \quad \mathbf{F}_k = \frac{\partial f}{\partial \mathbf{x}}\bigg|_{(\mathbf{x}_k, \mathbf{u}_k)}. \tag{13}$$

Also, $\tilde{\mathbf{x}} = \mathbf{x} - \hat{\mathbf{x}}$ is the error from the Taylor series expansion. The EKF algorithm has two main steps: prediction and update.

1) EKF Prediction Phase: Given a previous state estimate $\hat{\mathbf{x}}_{k-1|k-1}$, the *a priori* estimate is defined as

$$\hat{\mathbf{x}}_{k|k-1} = f(\hat{\mathbf{x}}_{k-1|k-1}, \mathbf{u}_k) \tag{14}$$

and the estimation error is

$$\begin{aligned} \tilde{\mathbf{x}}_{k|k-1} &\triangleq \hat{\mathbf{x}}_{k|k-1} - \mathbf{x}_k \\ &= f(\hat{\mathbf{x}}_{k-1|k-1}, \mathbf{u}_k) - f(\mathbf{x}_{k-1}, \mathbf{u}_k) - \mathbf{q}_k \\ &\approx \mathbf{F}_k \tilde{\mathbf{x}}_{k-1|k-1} - \mathbf{q}_k. \end{aligned} \tag{15}$$

The *a priori* covariance error is then calculated as

$$\begin{aligned} \mathbf{P}_{k|k-1} &= \mathbb{E}\big[\tilde{\mathbf{x}}_{k|k-1} \tilde{\mathbf{x}}_{k|k-1}^\top\big] \\ &= \mathbf{F}_k \mathbf{P}_{k-1|k-1} \mathbf{F}_k^\top + \mathbf{Q}_k \end{aligned} \tag{16}$$

2) EKF Update Phase: For the update phase, the measurement model is approximated by a linear system. The desired structure is given by

$$\hat{\mathbf{x}}_{k|k} = \hat{\mathbf{x}}_{k|k-1} + \mathbf{K}_k \big[\mathbf{z}_k - h(\hat{\mathbf{x}}_{k|k})\big]. \tag{17}$$

Considering that the *a priori* estimate error is uncorrelated with the measurement noise, the *a posteriori* covariance is obtained by

$$\mathbf{P}_{k|k} = \mathbf{P}_{k|k-1} + \mathbf{K}_k \mathbb{E}\big[\big(h(\mathbf{x}_k) - \mathbb{E}\big[h(\mathbf{x}_k)\big]\big)\tilde{\mathbf{x}}_{k|k-1}^\top\big] \tag{18}$$

As in the prediction phase, $\mathbf{h}(\mathbf{x}_k)$ is linearized through Taylor series expansion around $\hat{\mathbf{x}}_{k|k-1}$ to obtain

$$h(\mathbf{x}_k) \approx h(\hat{\mathbf{x}}_{k|k-1}) - \mathbf{H}_k \tilde{\mathbf{x}}_{k|k-1} \tag{19}$$

Equation (18) is then rewritten as

$$\mathbf{P}_{k|k} = \mathbf{P}_{k|k-1} + \mathbf{K}_k \mathbf{H}_k \mathbf{P}_{k|k-1} = (\mathbf{I} - \mathbf{K}_k \mathbf{H}_k)\mathbf{P}_{k|k-1} \tag{20}$$

and the Kalman gain is given by

$$\mathbf{K}_k = \mathbf{P}_{k|k-1} \mathbf{H}_k^T (\mathbf{H}_k \mathbf{P}_{k|k-1} \mathbf{H}_k^T + \mathbf{R}_k)^{-1} \tag{21}$$

To predict the system state using the EKF filter, it is sufficient to know the initial estimate and covariance, $\mathbf{x}_0$ and $\mathbf{P}_0$, the noise covariance, $\mathbf{Q}_i$, and the state transition model. The estimation process is initialized with the vehicle on the surface where it is possible to use GPS and the covariance matrix $\mathbf{P}_0$ is initialized based on sensor uncertainties. When the vehicle is underwater, the state is updated by dead-reckoning assuming that an SDUE map is provided. The initial state of the system is given by $\mathbf{x}_0 = (x_0, y_0, l_0, \psi_0, v_0)^\top$ and the covariance is initialized as $\mathbf{P}_0 = \mathbf{I}_{5\times5}$.

The EKF requires the additional calculation of the Jacobian of the state transition function $\mathbf{F}_k$ and the Jacobian of the observation model $\mathbf{H}_k$. The EKF procedure to compute the state estimate is described in Algorithm 1, which is called at each timestep of the simulation.

```
Algorithm 1 EKF($\hat{\mathbf{x}}_{k-1|k-1}, \mathbf{P}_{k-1|k-1}, \mathbf{z}_k$)
Input: $\hat{\mathbf{x}}_{k-1|k-1}$: current state estimate, $\mathbf{P}_{k-1|k-1}$: covariance matrix, $\mathbf{z}_k$: current measurement vector
Initialization: $\hat{\mathbf{x}}_{0|k} \in \mathbb{R}^d$, $\mathbf{P}_{0|k} \in \mathbb{R}^{d\times d}$
  Prediction
  $\hat{\mathbf{x}}_{\mathbf{k|k-1}} = f(\hat{\mathbf{x}}_{k-1|k-1}, \mathbf{u}_{k-1|k-1}) + \mathbf{q}_{k-1|k-1}$
  $\mathbf{F}_k = \frac{\partial f}{\partial \mathbf{x}}\Big|_{\hat{\mathbf{x}}_{k-1|k-1}}$
  $\mathbf{P}_{k|k-1} = \mathbf{F}_k \mathbf{P}_{k-1|k-1} \mathbf{F}_k^\top + \mathbf{Q}_k$
  Update
  $\mathbf{H}_k = \frac{\partial h}{\partial \mathbf{x}}\Big|_{\hat{\mathbf{x}}_{k|k-1}}$
  $\mathbf{K}_k = \mathbf{P}_{k|k-1} \mathbf{H}_k^\top \big(\mathbf{H}_k \mathbf{P}_{k|k-1} \mathbf{H}_k^\top + \mathbf{R}_k\big)^{-1}$
  $\hat{\mathbf{x}}_{k|k} = \hat{\mathbf{x}}_{k|k-1} + \mathbf{K}_k(\mathbf{z}_k - h_k(\hat{\mathbf{x}}_{k|k}))$
  $\mathbf{P}_{k|k} = \big(\mathbf{I} - \mathbf{K}_k \mathbf{H}_k\big)\mathbf{P}_{k|k-1}$
  return $\hat{\mathbf{x}}_{k|k}, \mathbf{P}_{k|k}$
```

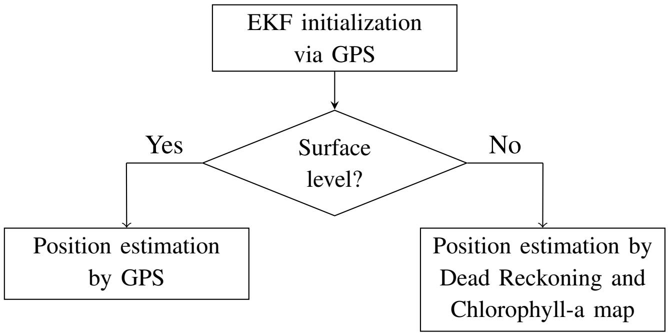
EKF initialization via GPS
Surface level?
Yes
No
Position estimation by GPS
Position estimation by Dead Reckoning and Chlorophyll-a map

Fig. 2. EKF Framework

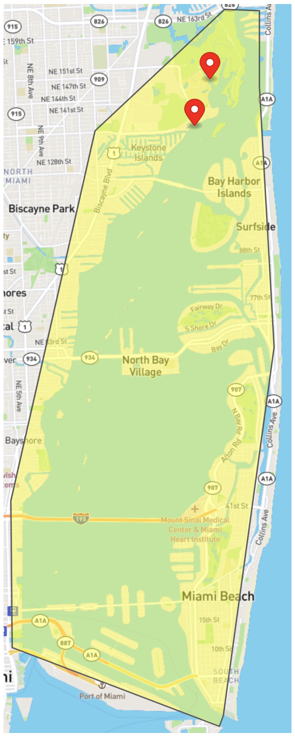

Fig. 3. Ocean work environment with mission locations

Problem 2: *Given an ocean work environment $\mathcal{W}$, an SDUE $\mathcal{S}$, and the desired trajectory τ, compute an estimated trajectory $\hat{\tau}$ that minimizes the tracking error.*

IV. METHODS

A. Data Collection

We begin by deploying a USV on a data collection mission. The in-situ data collected β_u is the ground truth for the labeling of the remote sensing data ρ. Figure 3 depicts our ocean work environment $\mathcal{W}$ with two markers representing the locations in-situ data on January 27th, 2022. The USV deployed is a YSI HYCAT that can measure several water quality parameters and is shown in Figure 4a and the areas in which in-situ data were collected are shown in Figure 4b.

Next, we create a satellite configuration that requests an S2 scene captured on the day closest to the in-situ collection date

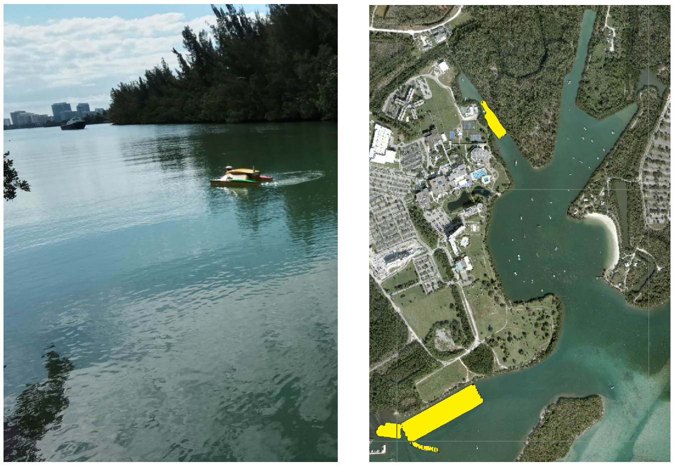

(a) (b)

Fig. 4. Data collection mission. (a) The USV deployed on a data collection mission (b) The lines where in-situ data were collected are shown in yellow

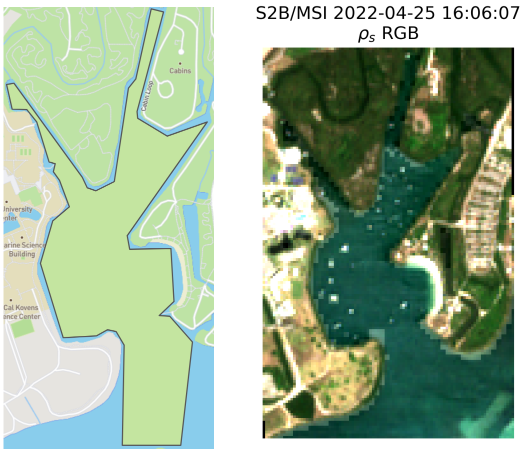

(a) (b)

Fig. 5. Remote sensing data retrieval. (a) The AOI as a bounding convex polygon within the ocean work environment; (b) A recent True Color (RGB) S2 image of the AOI with 10-meter pixel resolution and atmospherically corrected via ACOLITE.

with minimal cloud contamination and all available bands and metadata information over $\mathcal{W}$. In our case, we download an S2 scene of the Biscayne Bay captured on January 30th, 2022 with 0% cloud coverage. Figure 5a shows the AOI as $\mathcal{P}$ and Figure 5b depicts the AOI rendered using the red, green, and blue (RGB) bands of an S2 scene.

B. Data Processing

The Bathymetry measurements are corrected using NOAA tide information and the magnetic declination of the area. The S2 image is processed via the ACOLITE atmospheric correction application with sun glint correction enabled. The corrected scene is then loaded into the ESA Sentinel Application Platform (SNAP) to mask pixels with land, calculate indices, and extract pixels where in-situ data were calculated. We calculate NDCI and pSDB to be labeled with chlorophyll-a and bathymetry in-situ data respectively. The in-situ data is co-located with the remote sensing data using the SNAP Pixel extraction tool and is used to train two linear regression models to predict chlorophyll-a and bathymetry. Pixels that are contaminated by land are filtered out. To reduce the effects of outliers, the S2 10m resolution ensures that each pixel is co-located with multiple in-situ measurements. Negative estimates are replaced with the minimum positive in-situ measurement. Another satellite query configuration is then created to request the latest S2 scene available over $\mathcal{P}$. The second image is then corrected with ACOLITE before calculating the indices. The NDCI and pSDB calculated for each pixel are used as the input for the models to predict the surface level chlorophyll-a and bathymetry. To create the SDUE and solve *problem 1*, we use a simple exponential decay function to predict chlorophyll-a measurement of the layers below the surface level up to the maximum predicted depth.

V. RESULTS

A. Predictions

TABLE I
IN-SITU DATA COLLECTED

Water Parameter	Instrument	In-situ Samples
Bathymetry	SonTek HydroSurveyor M9	3893*
Chlorophyll-a	YSI EXO2 Sonde	3802*

*Unprocessed and collected across two missions carried out on January 27th, 2022.

TABLE II
CO-LOCATED DATA

Water Parameter	Count	Min	Max	Mean	Negative*
Bathymetry	3671	0.92	7.01	3.97	0
Chlorophyll-a	3600	0.05	5.68	1.83	1

*Number of negative in-situ data values.

Table I shows the number of in-situ bathymetry and chlorophyll-a samples collected. Table II shows the number of in-situ samples that were co-located to remote sensing data of water that is not contaminated by land along with a basic statistical analysis. Figure 6 shows the predicted bathymetry given the S2 image captured on April 25th, 2022 shown in Figure 5b. Land pixels default to 0. Water pixels predicted to have negative water depth are set to a depth of one while pixels that were predicted to be too deep were set to the largest in-situ sample found incremented by one. Most water pixels with outlier estimates are from small bodies of water outside of $\mathcal{P}$ or close to many land pixels. In Figure 5b, the deepest predicted depths are the corrected pixels on the bottom left and top right which appear to be artifacts from atmospheric correction and are actually land pixels. Most water pixels are predicted to be over three meters deep. The closer the pixels are to the land, the more likely the predicted depth is about one to two meters deep. Figure 7 shows the predicted Chlorophyll-a levels of the first four layers of the SDUE.

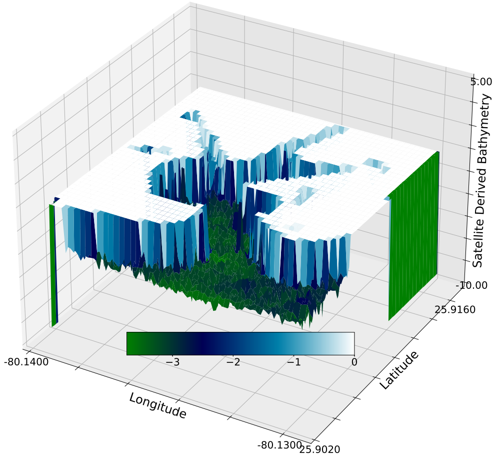

Fig. 6. Satellite-Derived Bathymetry

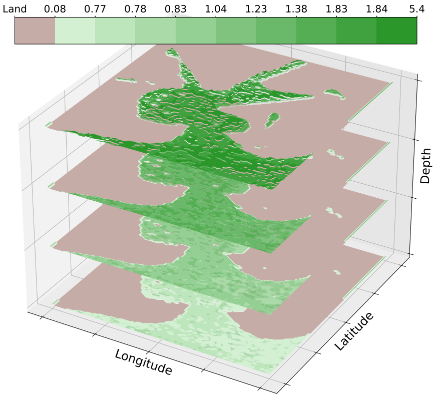

Fig. 7. Satellite-Derived Chlorophyll-a in the SDUE

B. Path Tracking Simulation

In this section, we propose two different vehicle trajectories based on the framework presented in Figure 2. For simulation purposes, we consider that the GPS signal is no longer available below 30 cm from the surface in both scenarios. The first desired trajectory is presented in Figure 8 (a). The vehicle moves at a constant forward speed at surface level for half of the simulation time and then it goes underwater in a sinusoidal descent for the rest of the simulation until reaching 5 meters deep. The dead-reckoning position error and EKF-based estimation error are shown in Figures (c) and (d), respectively. As we expected, the EKF-based approach minimizes the tracking error not only at the surface level but also underwater with the chlorophyll-a SDUE map information when compared to dead-reckoning tracking. The second desired trajectory is presented in Figure 8e. In this scenario, the heading angle is kept constant for the entire simulation while the vehicle moves at a constant forward speed and performs a sinusoidal path. Again, the EKF-based approach minimizes the tracking error when compared to dead-reckoning.

VI. CONCLUSIONS AND FUTURE WORK

The results reported are based on actual ocean model prediction data that demonstrate the applicability of our method. We co-located remote-sensing and in-situ data and applied it to a robot localization and navigation problem using a supervised machine learning model and EKF solution. With the available in-situ data, the SDB predictions are able to show a downward trend the closer a water pixel is to a land pixel. The model can be further improved by gathering additional in-situ samples of deeper waters in $\mathcal{W}$, incorporating higher resolution hyperspectral data and spectral unmixing in real time [10], making adjustments to the indices and masks used, changing Chlorophyll-a to one or more water parameters, leveraging other water quality measurements for estimate correction [7], and other avenues.

VII. ACKNOWLEDGMENT

This work is supported in part by the NSF grants IIS-2034123, IIS-2024733, the U.S. Dept. of Homeland Security grant 2017-ST-062000002, the National GEM Consortium, the Office of Naval Research, and the ESA Network of Resources Initiative. We also acknowledge the equipment loan from the Florida International University Institute of Environment, Miami, FL.

REFERENCES

[1] S. Balasubramanian, A. Rajput, R. W. Hascaryo, C. Rastogi, and W. R. Norris, "Comparison of Dynamic and Kinematic Model Driven Extended Kalman Filters (EKF) for the Localization of Autonomous Underwater Vehicles," tech. rep., 2021.

[2] M. H. Gholizadeh, A. M. Melesse, and L. Reddi, "A comprehensive review on water quality parameters estimation using remote sensing techniques," 2016.

[3] M. Nazeer, M. Bilal, M. M. Alsahli, M. I. Shahzad, and A. Waqas, "Evaluation of empirical and machine learning algorithms for estimation of coastal water quality parameters," *ISPRS International Journal of Geo-Information*, vol. 6, no. 11, 2017.

[4] S. Hafeez, M. Wong, H. Ho, M. Nazeer, J. Nichol, S. Abbas, D. Tang, K. Lee, and L. Pun, "Comparison of Machine Learning Algorithms for Retrieval of Water Quality Indicators in Case-II Waters: A Case Study of Hong Kong," *Remote Sensing*, vol. 11, no. 6, 2019.

[5] R. C. Cruz, P. R. Costa, S. Vinga, L. Krippahl, and M. B. Lopes, "A review of recent machine learning advances for forecasting harmful algal blooms and shellfish contamination," 2021.

[6] I. Caballero and R. P. Stumpf, "Retrieval of nearshore bathymetry from sentinel-2a and 2b satellites in south florida coastal waters," *Estuarine, Coastal and Shelf Science*, vol. 226, p. 106277, 2019.

[7] I. Caballero, R. P. Stumpf, and A. Meredith, "Preliminary assessment of turbidity and chlorophyll impact on bathymetry derived from sentinel-2A and sentinel-3A satellites in South Florida," *Remote Sensing*, vol. 11, no. 6, 2019.

[8] S. Mishra and D. R. Mishra, "Normalized difference chlorophyll index: A novel model for remote estimation of chlorophyll-a concentration in turbid productive waters," *Remote Sensing of Environment*, vol. 117, 2012.

[9] I. Caballero, R. Fernández, O. M. Escalante, L. Mamán, and G. Navarro, "New capabilities of Sentinel-2A/B satellites combined with in situ data for monitoring small harmful algal blooms in complex coastal waters," *Scientific Reports*, vol. 10, no. 1, 2020.

[10] S. Kodgule, A. Candela, and D. Wettergreen, "Non-myopic Planetary Exploration Combining in Situ and Remote Measurements," in *IEEE International Conference on Intelligent Robots and Systems*, 2019.

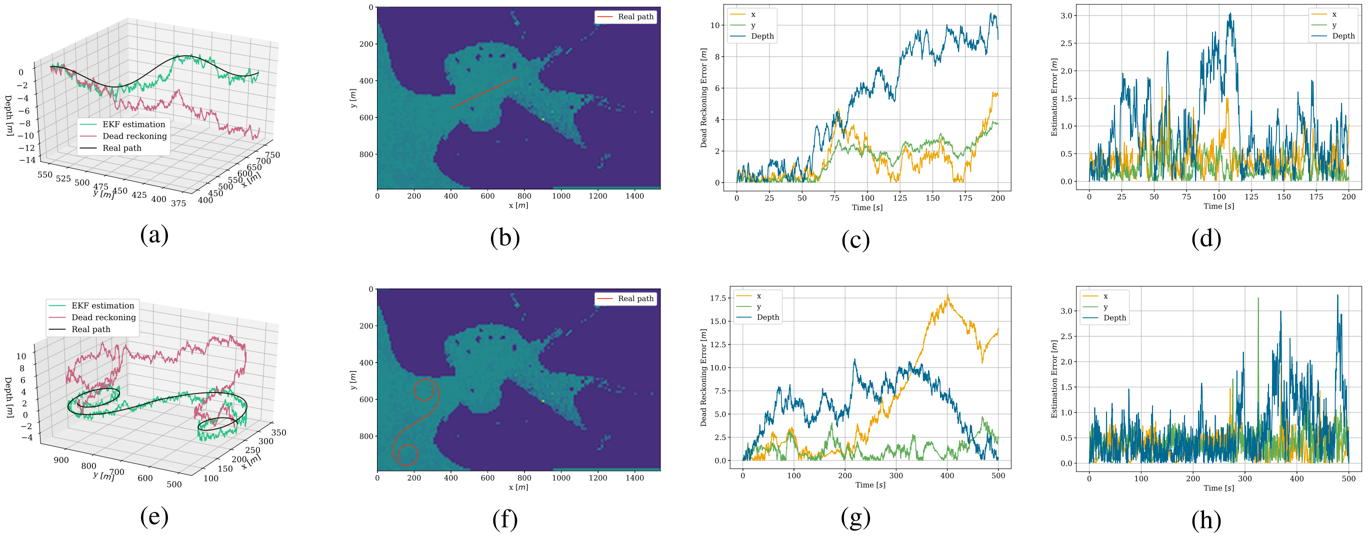

Fig. 8. EKF-based trajectory tracking using satellite-derived underwater environment map. (a), (e) Vehicle desired, estimated and dead-reckoning trajectories. (b), (f) Top view of the desired trajectories within the SDUE map. (c), (g) Dead reckoning position errors. (d), (h) EKF-based estimation errors.

[11] L. Paull, S. Saeedi, M. Seto, and H. Li, "Auv navigation and localization: A review," *IEEE Journal of Oceanic Engineering*, vol. 39, no. 1, pp. 131–149, 2014.

[12] R. T.N, A. Nherakkol, and G. Navelkar, "Navigation of autonomous underwater vehicle using extended kalman filter," in *Trends in Intelligent Robotics* (P. Vadakkepat, J.-H. Kim, N. Jesse, A. A. Mamun, T. K. Kiong, J. Baltes, J. Anderson, I. Verner, and D. Ahlgren, eds.), (Berlin, Heidelberg), pp. 1–9, Springer Berlin Heidelberg, 2010.

[13] P. Corke, C. Detweiler, M. Dunbabin, M. Hamilton, D. Rus, and I. Vasilescu, "Experiments with underwater robot localization and tracking," in *Proceedings 2007 IEEE International Conference on Robotics and Automation*, pp. 4556–4561, 2007.

[14] A. Kim and R. M. Eustice, "Real-time visual slam for autonomous underwater hull inspection using visual saliency," *IEEE Transactions on Robotics*, vol. 29, no. 3, pp. 719–733, 2013.

[15] I. Mahon, S. B. Williams, O. Pizarro, and M. Johnson-Roberson, "Efficient view-based slam using visual loop closures," *IEEE Transactions on Robotics*, vol. 24, no. 5, pp. 1002–1014, 2008.